Kinetic and equilibrium adsorption parameters estimation based on a heterogeneous intraparticle diffusion model

Luís M.S. Silva, Maria J. Muñoz-Peña,
Joaquín R. Domínguez-Vargas, Teresa González,
Eduardo M. Cuerda-Correa

PII: S2468-0230(20)30783-5
DOI: https://doi.org/10.1016/j.surfin.2020.100791
Reference: SURFIN 100791

To appear in: *Surfaces and Interfaces*

Received date: 6 July 2020
Revised date: 6 October 2020
Accepted date: 2 November 2020

Please cite this article as: Luís M.S. Silva, Maria J. Muñoz-Peña, Joaquín R. Domínguez-Vargas, Teresa González, Eduardo M. Cuerda-Correa, Kinetic and equilibrium adsorption parameters estimation based on a heterogeneous intraparticle diffusion model, *Surfaces and Interfaces* (2020), doi: https://doi.org/10.1016/j.surfin.2020.100791

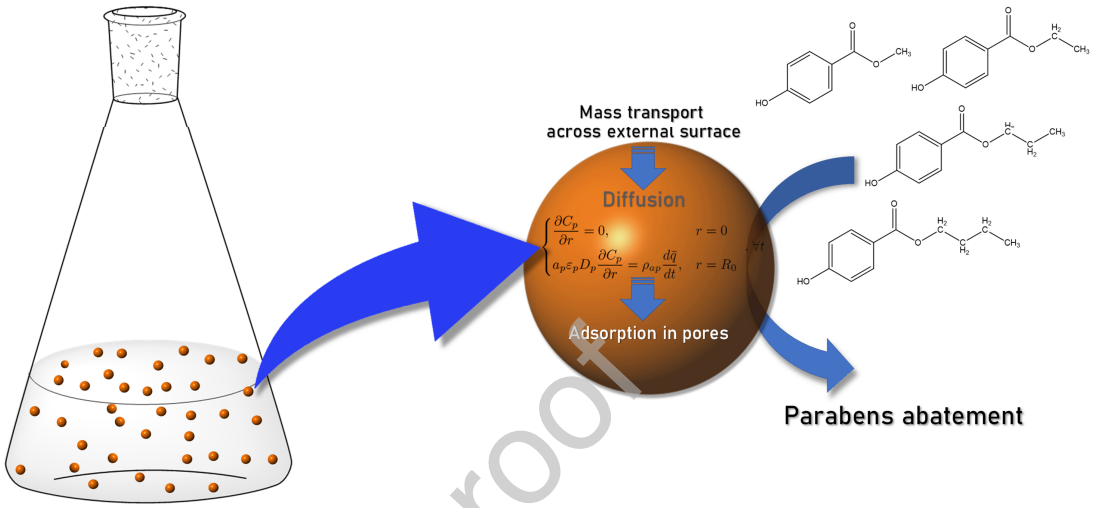

Kinetic and equilibrium adsorption parameters estimation based on a heterogeneous intraparticle diffusion model

Luís M. S. Silva[a], Maria J. Muñoz-Peña[b], Joaquín R. Domínguez-Vargas[b], Teresa González[b], Eduardo M. Cuerda-Correa[c,*]

[a] *CIETI, ISEP-School of Engineering, Polytechnic of Porto, Rua Dr. António Bernardino de Almeida, 431, 4249-015 Porto, PORTUGAL*
[b] *Department of Chemical Engineering and Physical Chemistry. Area of Chemical Engineering. Faculty of Sciences, University of Extremadura, Avda. de Elvas, s/n, E-06006. Badajoz, SPAIN*
[c] *Department of Organic and Inorganic Chemistry. Faculty of Sciences, University of Extremadura, Avda. de Elvas, s/n, E-06006 Badajoz, SPAIN*

Abstract

In this work, a commercial resin with a well-developed internal pore structure was chosen to adsorb four parabens used as probe molecules. The main novelty was to propose and validate a phenomenological transient adsorption model based on conservation law in both phases coupled with LangmuirâĂŹs equilibrium law and FickâĂŹs mass transfer rate law inside the pores. With such an aim, a heterogeneous three-parameter intraparticle diffusion model, IPDM, was formulated, and its numerical solution was fitted to time-dependent concentration data by minimizing the sum of squared residuals. Equilibrium constants were also predicted by fitting Langmuir isotherm to equilibrium data. A monolayer capacity of 0.81 mmol/g was calculated for the four parabens regardless of the number of carbons in the ester group. With the optimal parameters values from the IPDM fitting process, a system of ODEs comprising local sensitivity coefficients as dependent variables was solved to compute the parametersâĂŹ variance-covariance matrix and infer their ranges for a 95% marginal confidence interval. In order to test the validity of the proposed model, an attempt to

*corresponding author
Email address: emcc@unex.es (Eduardo M. Cuerda-Correa)

crosscheck between the parameters obtained by the estimation of the equilibrium related parameter, κ, and the modified capacity parameter, ξ'_p, and the ones obtained by fitting the LangmuirâĂŹs isotherm to equilibrium data was carried out. As far as equilibrium related parameters concern, there is a relative agreement inside the limits of the confidence range between the estimated values of the amount adsorbed in equilibrium with initial bulk solution concentration, q_0, and LangmuirâĂŹs equilibrium constant, K, adjusted to kinetic and equilibrium data, independently. Additionally, the order of magnitude of pore diffusivity obtained in this work is in accordance with the one predicted by Wilke-Chang correlation and is inversely proportional to the van der Waals volume raised to the power 0.53 in close agreement with the literature.

Keywords: Parabens adsorption, intraparticle diffusion model, partial differential equation, method of lines, parameter estimation, sensitivity analysis

1. Introduction

Although sorption processes are widely used, namely in water treatment, their modeling is still far from being reliable [1]. Generally, adsorption kinetic models can be divided into two main groups: adsorption reaction and adsorption diffusion models [2, 3]. Belonging to the former group are the widely used pseudo first and second-order models to adjust batch kinetic data [4–6] without any concern about the mechanism of adsorption in a purely empirical fitting exercise [7]. These are simple equations based on adsorption capacity which depend on experimental conditions and therefore lacks in the prediction on other not tested conditions. Conversely, adsorption diffusion models are based on mass conservation and kinetic and equilibrium laws independent from the experimental apparatus and so, predictive by nature.

As far as the adsorption diffusion model is concerned, several solutions may be found depending on the assumptions imposed. It is most often assumed that one of the three steps of the sorption process namely: 1) diffusion across the

film around the particles; 2) diffusion of adsorbate inside the pores and; 3) surface adsorption, controls the overall rate of adsorption [8, 9]. If extremely low adsorbate concentrations remain in the solutions, intraparticle diffusion progressively starts to slow down [10, 11]. In general, a well-agitated batch container assures that external resistance may be neglected. So, regarding that equilibrium between the adsorbate in the solid surface and solute in the fluid inside the pores is instantaneous then only the intraparticle diffusion rate-controlling models remain[10, 12].

Among the sorption systems controlled by mass transport of solute inside the particle, the *homogeneous solid diffusion model* (HSDM) is the simplest one [13]. This model does not distinguish between diffusion in the pores, diffusion along the surface subsequent the adsorption, or bulk diffusion inside the solid. The solid is treated as an amorphous and homogeneous isotropic particle. Barrer [14] solved analytically the resultant particle differential mass balance, providing that the fluid phase concentration remains constant, in a so-called "infinite" bath, and film mass transfer resistance is negligible. Boyd et al.[15] went further when they picked the concentration profile function of time and spherical radius and computed the total amount adsorbed at any instant and, with that, could manage to relate with the monitored bulk fluid concentration.

On the contrary, when the model deals with both diffusion in the pores and on its inner surface, it is commonly referred to as *pore volume and surface diffusion*, PVSD, model [16, 17]. When pore diffusion is negligible the model is simply called surface diffusion model, SD, and, in the other extreme, when surface diffusion is negligible, the PVSD is simplified to the pore volume diffusion (PVD) model. In this work, the solid particle was modeled as a two-phase particle medium in a so-called heterogeneous intraparticle diffusion model, IPDM, much alike the PVD model. Yet, there is a difference between the two models concerning the boundary condition used at the outer surface. In the later, it is assumed that the mass transported across the ïňĄlm matches the mass that crosses the external surface by diïňĂusion. In the present model, as stated in several papers [18–23], the difference between the mass of the adsorbate which

enters and exits a control volume by diffusion along the pores matches the accumulation of adsorbate in adsorbed plus fluid phases inside the pores of that given volume. Furthermore, the mass balance to the batch container must assure that the amount of adsorbate that accumulates inside the solid equals the depletion of solute in the bulk of fluid [18], representing a system where the solute in the fluid phase is "finite". Two boundary conditions were considered in the particle mass balance: one was the symmetry condition at the center of the sphere and the other was the interface transport condition [24] stating that adsorbate which passes across the outer surface of the particle by diffusion equals the total amount accumulated inside the particle whatever is the phase that the adsorbate can be present inside the particle, viz., adsorbed or in pore volume solution.

Langmuir adsorption isotherm has been commonly used to fit experimental data of the adsorption equilibrium of different pollutants with satisfactory results [25]. Particularly, Alwood *et al.* [26] made a comparison analysis between the first four esters of p-hydroxybenzoic acid similar to the one that was done in this work. Luo *et al.* [27] analyzed kinetic data, though testing pseudo-first and pseudo-second orders adsorption rate models only.

The main objective -and the principal novelty, too- of this work was to fit the numerical solution of the IPDM model coupled with Langmuir's equilibrium model to kinetic data obtained in a perfectly mixed batch container by computing the optimal model parameters that minimize the sum of squared residuals, SSR. To the best of the authors' knowledge, this approach was never attempted before. Additionally, the standard errors in the parameters were predicted to get information on how trustworthy the estimated parameters are. For this purpose, a sensitivity analysis was carried out.

To validate the model, equilibrium parameters included in the three-parameter IPDM model were compared with the ones estimated by nonlinear regression of equilibrium data. Furthermore, the molecular diffusivities predicted by the model were checked against the correlation of Wilke and Chang [28] for dilute solutions. The set of kinetic and equilibrium results got together from the four

parabens also contributed to confirm the consistency of the IPDM model proposed in this work, and the phenomenological approach contributes to greatly simplifying the model [23, 29].

2. Materials and methods

Resin DOWEX^{TM} OPTIPORE^{TM} L493 was provided by Sigma-Aldrich (Spain). The resin is a styrenic polymer highly cross-linked with divinylbenzene that is insoluble in strong acid, strong base, and organic solvents. It has a high surface area and a unique pore size distribution. Its pore volume is 1.16 $cm^3\ g^{-1}$, and its BET surface area is 1100 $m^2\ g^{-1}$. These adsorbents can be produced in both a wet and dry form. The wet material, L493, is intended for liquid applications while the dry form, V493, is used for gas adsorption. The typical properties of the two forms are shown in Table 1. This kind of polystyrenic resins have been widely used to adsorb different pollutants from waters, as such or chemically modified [30, 31].

Taking the apparent density and pore volume of the dry form it was possible to estimate the particle porosity multiplying each other and getting the value of 0.394 close enough to the one reported in the literature, i.e., 0.35 [32]. Two steps are necessary to carry out the preparation of the resin, namely washing and drying. Regarding the washing, the resin is rinsed with ultrapure water in a glass column, since the resin was stored in Na_2CO_3 and NaCl brine for retarding bacterial growth. The resin is washed until the conductivity of the water at the column exit is about 0.7 $\mu S\ cm^{-1}$. Then, the resin is washed with methanol to facilitate drying. Finally, it is dried in an oven at 50 ℃ for about 48 hours.

Methylparaben, MP, ($C_8H_8O_3$), ethylparaben, EP, ($C_9H_{10}O_3$), propylparaben, PP, ($C_{10}H_{12}O_3$), and butylparaben, BP, ($C_{11}H_{14}O_3$) were provided by Sigma-Aldrich, Spain, of the highest purity available (>98%). The solution of four parabens (5 ppm each) were prepared using high purity water obtained from a Millipore Milli-Q^{TM} system. All reagents and solvents were of analytical reagent grade. The molecular structure and some physicochemical properties of

parabens are summarized in Table 2.

2.1. Adsorption studies

2.1.1. Adsorption isotherms

Adsorption isotherms were plotted by conducting experiments with different amounts of adsorbent, ranging from 10 to 70 mg. 250 mL of a solution containing 5 mg L^{-1} of each paraben was added. Runs were carried out in triplicate at 20 ℃ for a period of time long enough to complete the adsorption process and reach equilibrium.

2.1.2. Kinetic studies

To monitor the bulk concentration evolution with time, kinetic batch runs were also conducted. The temperature of solutions was kept constant at 20 ℃ with 50 mg of resin dipped in 250 mL of an aqueous solution of each paraben (5 mg L^{-1}). The solutions were magnetically stirred for 48 h and samples were taken at several instants of time. Solutions were kept in contact under shaking with the adsorbent for a time span necessary to reach equilibrium.

2.2. Analytical method

The adsorbate concentration in solution after each treatment time was determined by a spectrophotometric method, for all four compounds studied in this work. In all adsorption experiments, samples were analyzed by ultraviolet-visible spectrophotometry measured at λ=254 nm with the aid of a Thermo Scientific Evolution 300 spectrophotometer, provided with a 1 cm optical pathway quartz cell. Ultrapure-Milli-Q^{TM} water was used as a reference. According to the Beer-Lambert law, the absorbance is directly proportional to the concentration of the paraben in solution in the range comprised between 0.3 and 10 ppm.

3. Theory

3.1. Mathematical model

The model assumes that the system operates isothermally. Writing a mass balance to the adsorbate in a spherical shell if r and $r+dr$ are inner and outer radii of the adsorbent particle, respectively, results in:

$$\varepsilon_p \frac{\partial C_p}{\partial t} + \rho_{ap} \frac{\partial q}{\partial t} = \frac{1}{r^2} \frac{\partial}{\partial r} \left(\varepsilon_p D_p r^2 \frac{\partial C_p}{\partial r} \right) \tag{1}$$

where C_p and q are the adsorbate concentration in the pores and in adsorbed phase functions of time and position inside the particle. The particle properties ε_p and ρ_{ap} stand for porosity and apparent density, respectively, and D_p is the pore diffusivity based on the cross-sectional area of the particle, expressed as cm^2 of particle per second. In this model both, surface and solid diffusion are neglected.

The initial and boundary conditions needed to find a particular solution for the above equation are as follows:

$$C_p = \begin{cases} 0, & 0 \leq r < R_0 \\ C_0, & r = R_0 \end{cases}, t = 0 \tag{2}$$

where C_0 is the initial concentration in the bulk fluid given that external transport resistance is negligible and:

$$\begin{cases} \dfrac{\partial C_p}{\partial r} = 0, & r = 0 \\ a_p \varepsilon_p D_p \dfrac{\partial C_p}{\partial r} = \rho_{ap} \dfrac{d\bar{q}}{dt}, & r = R_0 \end{cases}, \forall t \tag{3}$$

In the system above the first equation satisfies the symmetry condition at the center of the particle. The second equation states that all adsorbate mass that passes through the external surface of the particle at radius R_0 by diffusion must accumulate inside the particle. The variable $\bar{q}$ represents the mean adsorbate concentration inside the particle's volume, V_p, including the one that is in the pores of the particle which is defined by the following equation:

$$\rho_{ap} \bar{q} = \frac{\int_0^{V_P} \left(\rho_{ap} q + \varepsilon_p C_p \right) dV}{V_p} \tag{4}$$

The parameter a_p in system 3 represents the surface area per unit volume of the particle.

The accumulation term of the boundary condition at the particle surface is related to the depletion of adsorbate at the fluid phase, represented by $\frac{dC}{dt}$, by writing a mass balance to a closed perfectly mixed system comprising both phases such as:

$$\varepsilon V \frac{dC}{dt} + (1-\varepsilon) V \rho_{ap} \frac{d\bar{q}}{dt} = 0 \tag{5}$$

where V stands for the total volume of solution plus solid particles and ε represents the void fraction of the system made up of solid dispersed within the liquid. Substituting this expression in the boundary condition of the outer particle surface (equation 3) results in:

$$\varepsilon \frac{dC}{dt} + \frac{3}{R_0} (1-\varepsilon) \varepsilon_p D_p \left. \frac{dC_p}{dr} \right|_{r=R_0} = 0 \tag{6}$$

with $a_p = {}^{3}/_{R_0}$ for spherical geometry. The concentration at the bulk phase, *C(t)*, is the same as the concentration at the external surface of the particle, $C_p(R_0,t)$ regardless of the instant of time provided that external resistance is negligible.

Introducing the dimensionless variables $x = {}^{C}/_{C_0}$, $x_p = {}^{C_p}/_{C_0}$, $y = {}^{q}/_{q_0}$, $\zeta = {}^{r}/_{R_0}$ and $\theta = {}^{t}/_{\tau_d}$, equation 1 assumes the following expression:

$$\frac{\varepsilon_p C_0}{\tau_d} \frac{\partial x_p}{\partial \theta} + \frac{\rho_{ap} q_0}{\tau_d} \frac{\partial y}{\partial \theta} = \frac{1}{\zeta^2} \frac{\partial}{\partial \zeta} \left(\frac{\varepsilon_p D_p C_0}{R_0^2} \zeta^2 \frac{\partial x_p}{\partial \zeta} \right) \tag{7}$$

with q_0 as the adsorbate concentration in equilibrium with the initial bulk concentration, C_0, and $\tau_d = {}^{R_0^2}/_{D_p}$ meaning the time constant for intraparticle diffusion. Dividing the equation above by ${}^{\varepsilon_p C_0}/_{\tau_d}$ results in:

$$\frac{\partial x_p}{\partial \theta} + \frac{\rho_{ap} q_0}{\varepsilon_p C_0} \frac{\partial y}{\partial \theta} = \frac{1}{\zeta^2} \frac{\partial}{\partial \zeta} \left(\zeta^2 \frac{\partial x_p}{\partial \zeta} \right) \tag{8}$$

In order to solve the partial differential equation (PDE) written above it must be ensured that only one dependent variable is accounted for the equation. Thus, assuming that solute molecules in the pores of the particle are in equilibrium with those adsorbed at the inner surface, the Langmuir isotherm can be the

equation needed to relate between the variables x_p and y of equation 8 starting with:

$$q = \frac{QKC}{1 + KC} \tag{9}$$

with the usual meaning for the Langmuir's parameters, Q and K. Dividing the expression above by its similar at initial conditions leads to:

$$y = \frac{\kappa x_p}{1 + (\kappa - 1)\, x_p} \tag{10}$$

where $\kappa = 1 + KC_0$. Taking the derivative:

$$\frac{\partial y}{\partial x_p} = \frac{\kappa}{\left[1 + (\kappa - 1)\, x_p\right]^2} \tag{11}$$

and applying the chain rule for computing the derivatives of the composition of two functions:

$$\frac{\partial y}{\partial \theta} = \frac{\partial y}{\partial x_p}\frac{\partial x_p}{\partial \theta} = \frac{\kappa}{\left[1 + (\kappa - 1)\, x_p\right]^2}\frac{\partial x_p}{\partial \theta} \tag{12}$$

and, finally, substituting the above expression in equation 8 one obtains the following:

$$\left\{\frac{\rho_{ap} q_0}{\varepsilon_p C_0}\frac{\kappa}{\left[1 + (\kappa - 1)\, x_p\right]^2} + 1\right\}\frac{\partial x_p}{\partial \theta} = \frac{1}{\zeta^2}\frac{\partial}{\partial \zeta}\left(\zeta^2 \frac{\partial x_p}{\partial \zeta}\right) \tag{13}$$

The final form of the particle mass balance is attained after defining a new dimensionless parameter, ξ'_p, named modified capacity parameter, as $\rho_{ap} q_0 / \varepsilon_p C_0$:

$$\left\{\frac{\xi'_p \kappa}{\left[1 + (\kappa - 1)\, x_p\right]^2} + 1\right\}\frac{\partial x_p}{\partial \theta} = \frac{1}{\zeta^2}\frac{\partial}{\partial \zeta}\left(\zeta^2 \frac{\partial x_p}{\partial \zeta}\right) \tag{14}$$

It is a three-parameter space-time equation with the following dimensionless initial and boundary conditions, respectively:

$$x_p = \begin{cases} 0, & 0 \le \zeta < 1 \\ 1, & \zeta = 1 \end{cases}, \theta = 0 \tag{15}$$

and:

$$\begin{cases} \dfrac{\partial x_p}{\partial \zeta} = 0, & \zeta = 0 \\ \dfrac{\partial x_p}{\partial \theta} + 3\dfrac{1 - \varepsilon}{\varepsilon}\varepsilon_p \dfrac{\partial x_p}{\partial \zeta} = 0, & \zeta = 1 \end{cases}, \forall \theta \tag{16}$$

where the condition at the outer surface of the particle derives directly from equation (6).

3.2. Numerical solution

Equation 14 is commonly coined as *diffusion equation* and belongs to the class of parabolic PDEs. Regarding solving numerically this equation, a second-order finite difference approximation of the radial coordinate was conducted transforming a single PDE in a system of ordinary differential equations (ODEs) with respect to time. The system of ODEs was solved by a 2$^{\text{nd}}$ and 3$^{\text{rd}}$ order pair Runge-Kutta implicit integration method available in MatLab^{TM}. The jacobian matrix of the problem was supplied for the reliability and efficiency of the solution [33]. Although MatLab^{TM} has a tool to solve one dimension parabolic-elliptic equations (*pdepe function*) by the method of lines (MOL), the discretization was set manually by the authors in accordance with:

$$\left\{\frac{\xi_p'\kappa}{\left[1+(\kappa-1)\,x_{p_i}\right]^2}+1\right\}\frac{dx_{p_i}}{d\theta}=\frac{x_{p_{i+1}}-2x_{p_i}+x_{p_{i-1}}}{\Delta\zeta^2}+\frac{2}{\zeta_i}\frac{x_{p_{i+1}}-x_{p_{i-1}}}{2\Delta\zeta}\;,2\le i\le N-1 \tag{17}$$

where i is an index designating a position along a grid in ζ, and $\Delta\zeta$ is the spacing in ζ along the grid. The discretization of equation 14 for the left end of the grid (i.e. i=1) reveals a singularity. By applying L'Hôpital's rule, indetermination is overcome and the following ODE is obtained:

$$\left\{\frac{\xi_p'\kappa}{\left[1+(\kappa-1)\,x_{p_1}\right]^2}+1\right\}\frac{dx_{p_1}}{d\theta}=3\frac{x_{p_2}-2x_{p_1}+x_{p_0}}{\Delta\zeta^2} \tag{18}$$

Notice that x_{p_0} is outside the grid, i.e., i=0 is a fictitious point. However, its value can be assigned by applying the symmetry condition at the center:

$$\left.\frac{\partial x_p}{\partial\zeta}\right|_{i=1}\cong\frac{x_{p_2}-x_{p_0}}{2\Delta\zeta}=0\;\Leftrightarrow\;x_{p_0}=x_{p_2} \tag{19}$$

Substituting the above condition on equation 18 the following result is obtained:

$$\left\{\frac{\xi_p'\kappa}{\left[1+(\kappa-1)\,x_{p_1}\right]^2}+1\right\}\frac{dx_{p_1}}{d\theta}=6\frac{x_{p_2}-x_{p_1}}{\Delta\zeta^2} \tag{20}$$

On the other extreme of the grid (i.e., i=N) the boundary condition resultant of the imposition that all solute that crosses the particle surface by diffusion accumulates inside the particle volume combined with a mass balance to the

batch system (second equation of the system 16) is discretized as follows:

$$\frac{dx_{p_N}}{d\theta} = -3\frac{1-\varepsilon}{\varepsilon}\varepsilon_p\frac{x_{p_N} - x_{p_{N-1}}}{\Delta\zeta} \tag{21}$$

The integration of equations 17, 20, and 21 gives the numerical solution $x_{p_1}(t)$, $x_{p_2}(t)$,...,$x_{p_N}(t)$ for a given set of parameters τ_d, ξ_p', and κ where x_p at the right end of the grid (i.e., i=N) is considered equal to the normalized concentration in the bulk phase.

The purpose of this work was to fit the numerical solution of dimensionless concentration at the outer surface of the particle, $x_{p_N}(t)$, to the normalized data set, C/C_0 by minimizing SSR. For the effect the function *fminsearch* available in MatLab^{TM} software based on the direct search nonlinear Nelder-Mead simplex technique was used.

3.3. Sensitivity analysis

A local sensitivity analysis was implemented to infer the standard error of the adjustable parameters for the two sets of experimental data: kinetics and equilibrium data.

Concerning kinetics data, it will be considered a system described by a set of N coupled differential equations containing m parameters:

$$\frac{d\mathbf{x_p}}{dt} = \mathbf{F}(\mathbf{x_p}, \mathbf{k}, t) \tag{22}$$

and the local sensitivity coefficient is defined as [34]:

$$s_j^{(i)}(t) = \frac{\partial x_{p_i}(t, \mathbf{k})}{\partial k_j} \tag{23}$$

which describes the change of a state variable x_{p_i} relatively to a change of parameter k_j [35] with $1 \leq i \leq$ N and $1 \leq j \leq$ m as a function of time t. In this case, in which the physical model is described by a set of ODEs, the sensitivity matrix $\underset{(N\times m)}{\mathbf{S}}(t)$ cannot be computed by a simple differentiation. Nevertheless, differentiating equation 22 with respect to $\mathbf{k}$ and applying chain rule results in:

$$\frac{d\mathbf{S}(t)}{dt} = \left(\frac{\partial \mathbf{F}^{\mathrm{T}}}{\partial \mathbf{x}}\right)^{\mathrm{T}}\mathbf{S}(t) + \left(\frac{\partial \mathbf{F}^{\mathrm{T}}}{\partial \mathbf{k}}\right)^{\mathrm{T}} \tag{24}$$

and, then, the sensitivity coefficients can be determined by applying the condition $\mathbf{S}(t{=}0){=}\mathbf{0}$ because initial conditions of the state variables are independent of the parameters vector $\mathbf{k}$ [36].

At the end of the least-squares optimization, the set of N state equations 17, 20, and 21 are, once again, solved simultaneously with sensitivity equations (24) in a total of $N{\times}(m{+}1)$ dimensional ODE system for the optimal values of vector $\mathbf{k}^* = \left[\tau_d^*, \xi_p'^*, \kappa^*\right]^{\mathrm{T}}$ with $m{=}3$.

When the purpose is to minimize SSR, the least-squares estimate $\mathbf{k}^*$ may be assumed to have a normal distribution, unbiased (i.e. $\mathrm{E}(\mathrm{k}^*){=}\mathrm{k}$) and, so, their variance-covariance matrix is given by:

$$Cov\left(\mathbf{k}^*\right) = \frac{SSR}{n-m}\left(\sum_{i=1}^{n}\mathbf{S}\left(t_i\right)^{\mathrm{T}}\mathbf{S}\left(t_i\right)\right)^{-1} \tag{25}$$

where n is the number of independent t data points and SSR is defined as usual, following the classical approach of Fisher-information-matrix [35]. Finally, a *100(1-α)%* marginal confidence interval can be inferred for each parameter k_j as follows:

$$k_j^* - \sqrt{Cov_{jj}\left(\mathbf{k}^*\right)}\cdot t_{1-\alpha/2,n-m} \le k_j \le k_j^* + \sqrt{Cov_{jj}\left(\mathbf{k}^*\right)}\cdot t_{1-\alpha/2,n-m} \tag{26}$$

where $t_{1-\alpha/2,n-m}$ is 1-α/2 critical value of the *Student's* t-distribution of n-m degrees of freedom.

For algebraic models $y = f\left(x, \mathbf{k}\right)$, such as adsorption equilibrium isotherms, sensitivity matrices are substituted by the jacobian, $\mathbf{J}$, in the calculation of variance-covariance of $\mathbf{k}^*$ as follows:

$$Cov\left(\mathbf{k}^*\right) = \frac{SSR}{n-m}\left(\mathbf{J}^{\mathrm{T}}\mathbf{J}\right)^{-1} \tag{27}$$

where each element of the $\mathbf{J}(n{\times}m)$ matrix is computed as $j_j^{(i)} = \dfrac{\partial f\left(x_i, \mathbf{k}\right)}{\partial k_j}$ for n equilibrium data points and m model parameters.

4. Results and discussion

The IPDM single resistance mass transfer model coupled with Langmuir isotherm described by equation 14 that satisfies the initial conditions set by

equation 15 and boundary conditions by equation 16 were solved numerically in each iteration of the optimization routine by applying the method of lines. For the effect, a discretization in space coordinate of 21 points distributed equidistantly was implemented as stated by equations 17, 20, and 21.

The equilibrium adjustable parameters resultant from the kinetic model, q_0 and K, were compared to the Langmuir constants obtained by nonlinear least-squares of equilibrium data. The equilibrium adjustable parameters resultant from the kinetic model, q_0 and K, were compared to the Langmuir constants obtained by nonlinear least-squares of equilibrium data.

4.1. Transient kinetic analysis

The optimal IPDM parameters values and their respective 95% marginal confidence range are presented in Table 3. Based on the values of coefficient of determination the model fits adequately the kinetic data. To support this claim, the dimensionless concentration profile inside the particle, x_p, was plotted along the normalized radius and dimensionless time, respectively, ζ and θ as shown in Figure 1. In the same plot at $\zeta = 1$ the adsorbate concentration data in the bulk fluid is also represented admitting that external diffusional fluid resistance is negligible. In supporting information, equivalent graphs are plotted for the other three parabens.

Despite the goodness of fit, the parameter κ associated to Langmuir's equilibrium constant, K, shows, in general, a significant uncertainty, not least because that a space-time model was used to fit a small number of data points corresponding to the normalized concentration at the outer surface of the particle only. As confirmed by Joshi *et al.* [35], the quality of the estimated parameters not only depends on the number of data points but also on the region where the experimental data is picked.

Another parameter estimated by the IPDM model was the time constant for intraparticle diffusion, τ_d. This allows to infer pore diffusivities for the four parabens and these, in turn, are related with binary diffusivity by the equation

[37]:

$$D_p = \frac{D_{AB}}{\tau} \tag{28}$$

where τ represents tortuosity. After plotting the inferred D_p versus binary diffusivity of each paraben at infinite dilution in water predicted by Wilke-Chang correlation with the molar volume of paraben at boiling point obtained by Le Bas method [38], some shreds of evidence must be highlighted.

As shown in Figure 2, the order of magnitude of the pore diffusivities is the same as the molecular diffusivities predicted by the Wilke-Chang correlation. As a general trend, pore diffusivity decreases as the number of carbons in the ester group increases. However, D_p is, on average, 46% greater than D_{AB} when the latter should be, in general, τ times greater than the former (see equation 28). In case that, in the absence of better information, tortuosity is estimated as the inverse of particle porosity then the molecular diffusivity calculated by equation 28 is overrated, being, on average, 3.7-fold greater than the one predicted by Wilke-Chang correlation. Yet, this does not detract credibility from the model as will be shown below.

With the aim to analyze the influence of the molecule stereochemistry in the intraparticle diffusivity a log-log graph representing D_p as a function of molecular volume, V_{vdW}, is represented in Figure 3. The molecular volume is computed as the volume enclosed by a sphere with the van der Waals radius determined by the Bondi method [39]. The weighted linear regression to this data discloses a proportionality between D_p and ${V_{vdW}}^{-0.53}$ which is in close agreement with the empirical relationship obtained by La-Scalea *et al.* [40] in their equation 12:

$$\log\left[D_{AB}\left(cm^2 s^{-1}\right)\right] = -3.96 - 0.52\log\left[V_{vdW}\left(\overset{\circ}{A}^3\right)\right] \tag{29}$$

However, this similarity is not conclusive since the slope of the solid line unveils a high uncertainty as shown in the expression embedded in Figure 3.

The IPDM model coupled with the Freundlich equilibrium model was also fitted to the same kinetic data giving always worse regressions. In supplemen-

tary material, the results obtained by the least-squares optimization are also presented.

4.2. Equilibrium analysis

The Langmuir's adjustable parameters obtained by nonlinear regression to experimental equilibrium data and respective 95% marginal confidence range are presented in Table 3. The experimental data and fitted Langmuir isotherms are also plotted in Figure 4. Although the relative position of adjusted lines may presume that the adsorbed quantity increases with the length of alkyl ester side-chain, the values of monolayer quantity estimated by the Langmuir model, Q, show otherwise. Thus, plotting in Figure 5 Q in $mmol\,g^{-1}$ versus the number of carbons in the ester group, it can be concluded by a weighted linear regression that the monolayer amount is about 0.81 mmol g^{-1} whatever the paraben is.

This evidence is in agreement with the work of Allwood [26]. This author concluded that the adsorptive capacity of the methyl, ethyl, propyl, and butyl esters of *p*-hydroxybenzoic acid by magnesium trisilicate do not depend on the molecular weight or the hydrophobicity of the molecule. It is proposed in the mentioned work that the adsorption must be a function of the aromatic core of the paraben rather than the alkyl ester side-chain. Also in Table 3 the values of q_0 corresponding to the equilibrium concentration C_0=5 ppm and respective 95% marginal confidence ranges are presented.

4.3. Crosscheck between adsorption isotherms and kinetic studies

Regarding the validation of the IPDM kinetic model coupled with the Langmuir equilibrium model to this system, the equilibrium constants inferred from the adjustable model parameters were compared to those obtained by fitting Langmuir isotherm to equilibrium data. In Figure 6 a) the values of the amount adsorbed of each paraben in equilibrium with the bulk concentration of 5 ppm, $q_{0\ kinetics}$, determined as of the estimated IPDM parameter ξ'_p, are plotted against $q_{0\ equilibrium}$ calculated from the Langmuir isotherm at the same equilibrium fluid concentration. It should be noted that the value obtained for

methylparaben by both routes is practically the same. In Figure 6 b) the values of $K_{kinetics}$ calculated from the estimated IPDM parameter κ are represented versus those predicted by Langmuir isotherm, $K_{equilibrium}$. The horizontal and vertical bars represent the standard errors of the estimated parameters calculated by the two sets of experiments, adsorption isotherms and kinetic studies, respectively. It is evident that the K values predicted by kinetic analysis are greater than the ones fitted to the equilibrium data. Even so, it is noteworthy that the K values for methyl and butylparaben are close enough to the diagonal line and the two more far away values (propyl and ethylparaben) placed in the upper half of the graph are also the same compounds which show q_0 values in the lower half of Figure 6 a) probably denouncing a compensation effect. In fact, granted that the monolayer capacity is constant for all parabens, expressing Langmuir isotherm as follows:

$$q_0 \frac{1 + KC_0}{KC_0} = Q = \text{constant} \tag{30}$$

when K increases, the amount adsorbed q_0 must decrease to keep constant the left-hand side of Equation 30.

5. Conclusions

In accordance with the experimental results obtained in this work, the following conclusions can be drawn:

- A heterogeneous single-resistance intraparticle diffusion model, IPDM, was proposed to describe the kinetics of adsorption of the first four alkyl esters of *p*-hydroxybenzoic acid by a commercial resin. A least-squares method was implemented to fit the numerical solution of the derived PDE equation that satisfy specific boundary and initial conditions to the bulk concentration data monitored in a batch container over time.

- Three parameters were estimated namely: time constant for intraparticle diffusion, τ_d [T], and the dimensionless modified capacity parameter, ξ_p',

and equilibrium constant related parameter, κ. A sensitivity analysis was then carried out and allowed to verify that the parameter κ is affected by a large uncertainty indicating that it does not have a significant influence in fitting the IPDM model to data collected at the bulk of the solution.

- In relation to the time constant estimation, values of pore diffusivity were inferred from and compared with binary diffusivity concluding that they are of the same order of magnitude. In addition, a linear trendline in the log-log scale between D_p and the molecular volume, V_{vdW}, was found for the four parabens tested in this work proving that the dimension of molecule influences the easiness of transport inside the pores of the adsorbate.

- The validation of the IPDM model coupled with Langmuir isotherm was conducted by comparing the values of the amount adsorbed in equilibrium with the initial bulk concentration of 5 ppm, q_0, and LangmuirâĂŹs equilibrium constant, K, obtained independently by the two sets of experiments, adsorption isotherms, and kinetic studies. A relative agreement was achieved. Concerning the parameters related to methylparaben, the match between the results obtained by the two routes of analysis is quite good. In the case of the ethyl and propylparaben, a kind of compensation effect between q_0 and K was observed. No valid conclusion can be drawn for butylparaben because of its parametersâĂŹ degree of uncertainty.

- To sum up, the IPDM model can correctly describe the kinetics of adsorption of the first four parabens by a commercial resin. This model and respective numerical method can set the basis to study the kinetics of any system that is governed by intraparticle pore diffusion.

Acknowledgments

The authors gratefully acknowledge financial support of this research work through the Comisión Interministerial de Ciencia y Tecnología (CICYT)-CTM2013-

41354-R and Fundação para a Ciência e a Tecnologia (FCT)-UIDB/04730/2020 projects.

References

References

[1] V. Russo, R. Tesser, M. Trifuoggi, M. Giugni, M. Di Serio, A dynamic intra-particle model for fluid-solid adsorption kinetics, Computers and Chemical Engineering 74 (2015) 66–74.

[2] H. Qiu, L. Lv, B.-C. Pan, Q.-J. Zhang, W.-M. Zhang, Q.-X. Zhang, Critical review in adsorption kinetic models, Journal of Zhejiang University: Science A 10 (2009) 716–724.

[3] C. Yao, T. Chen, A new simplified method for estimating film mass transfer and surface diffusion coefficients from batch adsorption kinetic data, Chemical Engineering Journal 265 (2015) 93–99.

[4] S. Azizian, Kinetic models of sorption: A theoretical analysis, Journal of Colloid and Interface Science 276 (2004) 47–52.

[5] W. Hassan, S. Noureen, M. Mustaqeem, T. Saleh, S. Zafar, Efficient adsorbent derived from haloxylon recurvum plant for the adsorption of acid brown dye: Kinetics, isotherm and thermodynamic optimization, Surfaces and Interfaces 20 (2020).

[6] A. Saravanan, S. Karishma, S. Jeevanantham, S. Jeyasri, A. Kiruthika, P. Kumar, P. Yaashikaa, Optimization and modeling of reactive yellow adsorption by surface modified delonix regia seed: Study of nonlinear isotherm and kinetic parameters, Surfaces and Interfaces 20 (2020).

[7] S. Douven, C. Paez, C. Gommes, The range of validity of sorption kinetic models, Journal of Colloid and Interface Science 448 (2015) 437–450.

[8] Y. Ho, J. Ng, G. McKay, Kinetics of pollutant sorption by biosorbents: Review, Separation and Purification Methods 29 (2000) 189–232.

[9] J. Wang, X. Guo, Adsorption kinetic models: Physical meanings, applications, and solving methods, Journal of Hazardous Materials 390 (2020).

[10] Z. Zhang, Z. Zhang, Y. Fernandez, J. Menendez, H. Niu, J. Peng, L. Zhang, S. Guo, Adsorption isotherms and kinetics of methylene blue on a low-cost adsorbent recovered from a spent catalyst of vinyl acetate synthesis, Applied Surface Science 256 (2010) 2569–2576.

[11] M. Saxena, N. Sharma, R. Saxena, Highly efficient and rapid removal of a toxic dye: Adsorption kinetics, isotherm, and mechanism studies on functionalized multiwalled carbon nanotubes, Surfaces and Interfaces 21 (2020).

[12] P. Ganguly, R. Sarkhel, P. Das, Synthesis of pyrolyzed biochar and its application for dye removal: Batch, kinetic and isotherm with linear and non-linear mathematical analysis, Surfaces and Interfaces 20 (2020).

[13] D. Cooney, Adsorption design for wastewater treatment, Lewis Publishers, Boca Raton, Fl, 1999.

[14] R. Barrer, Diffusion in and through solids, The University press; Macmillan, Cambridge, Eng.; New York, 1941.

[15] G. Boyd, A. Adamson, L. Myers Jr., The exchange adsorption of ions from aqueous solutions by organic zeolites. ii. kinetics, Journal of the American Chemical Society 69 (1947) 2836–2848.

[16] R. Leyva-Ramos, C. Geankoplis, Model simulation and analysis of surface diffusion of liquids in porous solids, Chemical Engineering Science 40 (1985) 799–807.

[17] R. Ocampo-Perez, R. Leyva-Ramos, P. Alonso-Davila, J. Rivera-Utrilla, M. Sanchez-Polo, Modeling adsorption rate of pyridine onto granular activated carbon, Chemical Engineering Journal 165 (2010) 133–141.

[18] C. Gomes, M. Almeida, J. Loureiro, Gold recovery with ion exchange used resins, Separation and Purification Technology 24 (2001) 35–57.

[19] J. Chen, S. Wu, Acid/base-treated activated carbons: Characterization of functional groups and metal adsorptive properties, Langmuir 20 (2004) 2233–2242.

[20] W. Plazinski, W. Rudzinski, A novel two-resistance model for description of the adsorption kinetics onto porous particles, Langmuir 26 (2010) 802–808.

[21] R. Garcia-Reyes, J. Rangel-Mendez, Adsorption kinetics of chromium(iii) ions on agro-waste materials, Bioresource Technology 101 (2010) 8099–8108.

[22] A. Hekmatzadeh, A. Karimi-Jashni, N. Talebbeydokhti, B. KlÃÿve, Adsorption kinetics of nitrate ions on ion exchange resin, Desalination 326 (2013) 125–134.

[23] V. Steffen, E. Antonio da Silva, L. Evangelista, L. Cardozo-Filho, Phenomenological adsorption isotherm for a binary system based on poissonâĂŞboltzmann equation, Surfaces and Interfaces 10 (2018) 50–57.

[24] T. Kawakita, H.-J. Fan, Y. Seida, J. Fujiki, E. Furuya, A simplified technique to determine intraparticle diffusivity of macro-reticular resins, Sustainable Environment Research 26 (2016) 249–254.

[25] F. Alakhras, E. Alhajri, R. Haounati, H. Ouachtak, A. Addi, T. Saleh, A comparative study of photocatalytic degradation of rhodamine b using natural-based zeolite composites, Surfaces and Interfaces 20 (2020).

[26] M. Allwood, The adsorption of esters of p-hydroxybenzoic acid by magnesium trisilicate, International Journal of Pharmaceutics 11 (1982) 101–107.

[27] H.-Y. Luo, M. Zhang, N.-C. Si, M.-J. Meng, L. Yan, W.-J. Zhu, C.-X. Li, Molecularly imprinted open porous membranes made from pickering w/o

hipes for selective adsorption and separation of methyl 4-hydroxybenzoate, Chinese Chemical Letters 26 (2015) 1036–1041.

[28] C. Wilke, P. Chang, Correlation of diffusion coefficients in dilute solutions, AIChE Journal 1 (1955) 264–270.

[29] V. Steffen, E. Silva, L. Evangelista, L. Cardozo-Filho, Debye-huckel approximation for simplification of ions adsorption equilibrium model based on poisson-boltzmann equation, Surfaces and Interfaces 10 (2018) 144–148.

[30] Y. Wang, B. Chi, M. Li, W. Wei, Y. Wang, D. Chen, Synthesis of sulfonated polystyrene sphere based magnesium silicate and its selective removal for bisphenol a, Surfaces and Interfaces 14 (2019) 9–14.

[31] A. Nathani, A. Adaval, A. Karim, C. Sharma, Poly(styrene-block-methylmethacrylate) derived electrospun mesoporous nanofibers, Surfaces and Interfaces 12 (2018) 168–178.

[32] C. Wegmann, E. Garcia, P. Kerkhof, Kinetics of acrylonitrile adsorption from an aqueous solution using dowex optipore l-493, Separation and Purification Technology 81 (2011) 429–434.

[33] L. Shampine, M. Reichelt, The matlab ode suite, SIAM Journal on Scientific Computing 18 (1997) 1–22.

[34] M. Haaker, P. Verheijen, Local and global sensitivity analysis for a reactor design with parameter uncertainty, Chemical Engineering Research and Design 82 (2004) 591–598.

[35] M. Joshi, A. Kremling, A. Seidel-Morgenstern, Model based statistical analysis of adsorption equilibrium data, Chemical Engineering Science 61 (2006) 7805–7818.

[36] P. Englezos, Applied parameter estimation for chemical engineers, Marcel Dekker, New York, 2001.

[37] C.-W. Hui, B. Chen, G. McKay, Pore-surface diffusion model for batch adsorption processes, Langmuir 19 (2003) 4188–4196.

[38] R. Reid, J. Prausnitz, B. Poling, The properties of gases and liquids, McGraw-Hill, New York ; London, 4th edition, 1987.

[39] A. Bondi, Van der waals volumes and radii, Journal of Physical Chemistry 68 (1964) 441–451.

[40] M. La-Scalea, C. Souza Menezes, E. Ferreira, Molecular volume calculation using am1 semi-empirical method toward diffusion coefficients and electrophoretic mobility estimates in aqueous solution, Journal of Molecular Structure: THEOCHEM 730 (2005) 111–120.

[41] R. Golden, J. Gandy, G. Vollmer, A review of the endocrine activity of parabens and implications for potential risks to human health, Critical Reviews in Toxicology 35 (2005) 435–458.

[42] M. Dymicky, C. Huhtanen, Inhibition of clostridium botulinum by p-hydroxybenzoic acid n-alkyl esters, Antimicrobial Agents and Chemotherapy 15 (1979) 798–801.

[43] M. O'Neil, The Merck index : an encyclopedia of chemicals, drugs, and biologicals, Merck, Whitehouse Station, N.J., 13th edition, 2001.

Table 1: Typical physical and chemical properties of DOWEX^{TM} OPTIPORE^{TM} L493 and V493

Property	L493	V493
Matrix structure	Macroporous styrenic polymer	Macroporous styrenic polymer
Physical form	Orange to brown spheres	Orange to brown spheres
Particle size (mesh)	20-50	20-50
Moisture content (%)	50-65	<5
BET surface area (m^2 g^{-1})	1100	1100
Pore volume (cm^3 g^{-1})	1.16	1.16
Average pore diameter (Å)	46	46
Apparent density (g cm^{-3})	0.62	0.34
Ash content (%)	<0.01	<0.01
Crush strength (g/bead)	>500	>500
Heat capacity (cal g^{-1} $^{\circ}C^{-1}$)	0.75	0.30
Thermal conductivity (cal s^{-1} cm^{-1} $^{\circ}C^{-1}$)	0.00033	0.00016

Table 2: Chemical formula and relevant physicochemical properties of parabens

Property	MP	EP	PP	BP
Chemical formula	$C_8H_8O_3$	$C_9H_{10}O_3$	$C_{10}H_{12}O_3$	$C_{11}H_{14}O_3$
Molecular weight[a] (g mol^{-1})	152.15	166.18	180.20	194.23
pK_a[b]	8.17	8.22	8.35	8.37
log K_{OW}[a]	1.66	2.19	2.71	3.24
Boiling point[c] (℃)	270-280*	297-298*	n.a.	n.a.
Solubility in water at 25 ℃[b] (g mL^{-1})$\times 10^2$	0.25	0.075	0.05	0.017
van der Waals volume (Å)**	135.76	152.62	169.57	186.53

n.a., not available

[a]Golden et al. [41]; [b]Dymicky and Huhtanen [42]; [c]The Merck Index [43].

* decomposes; ** calculated by ChemAxon.

Table 3: Parameters estimated and calculated from the former by kinetic studies and adsorption isotherms and respective 95% marginal confidence intervals for the 4 parabens: methylparaben, MP, ethylparaben, EP, propylparaben, PP, and butylparaben, BP

Adsorbate	Transient kinetic analysis - IPDM model						
	Estimated				Calculated		
	τ_d (s)	$\xi_p^{'} \times 10^{-3}$	$\kappa \times 10^{-2}$	R^2	$D_p \times 10^7$ (cm^2 s^{-1})	q_0 (mg g^{-1})	K (L mg^{-1})
MP	78.8±2.4	16.7±1.5	0.105±0.027	0.9987	103±3	97±9	1.9±0.5
EP	84.1±2.2	14.14±0.73	3.0±3.0	0.9989	97±3	82±4	60±59
PP	99.0±5.2	18.45±0.80	4.1±6.6	0.9969	82±4	107±5	82±132
BP	93.4±1.5	35±64	0.95±3.4	0.9997	87±1	204±368	19±70

Adsorbate	Equilibrium analysis - Langmuir isotherm				
	Estimated			Calculated	
	Q (mg g^{-1})	K (L mg^{-1})	R^2	q_0 (mg g^{-1})	
MP	121±61	0.9±1.0	0.8668	98±53	
EP	134±20	1.9±0.7	0.9790	121±19	
PP	182±62	1.5±1.1	0.9360	161±57	
BP	147±94	11±33	0.8694	145±92	

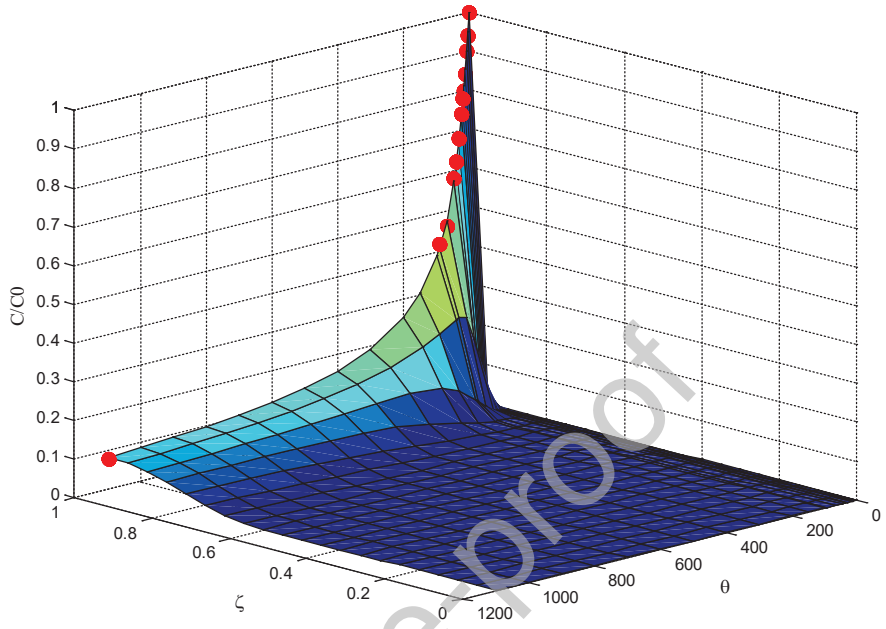

Figure 1: Methylparaben normalized concentration profile as a function of dimensionless time, θ, and radial normalized coordinate, ζ. Red dots represent experimental data. *Experimental conditions*: Temperature, 20 °C; mass of adsorbent, 50 mg; volume of solution, 250 mL; initial concentration of paraben, 5 mg L^{-1}.

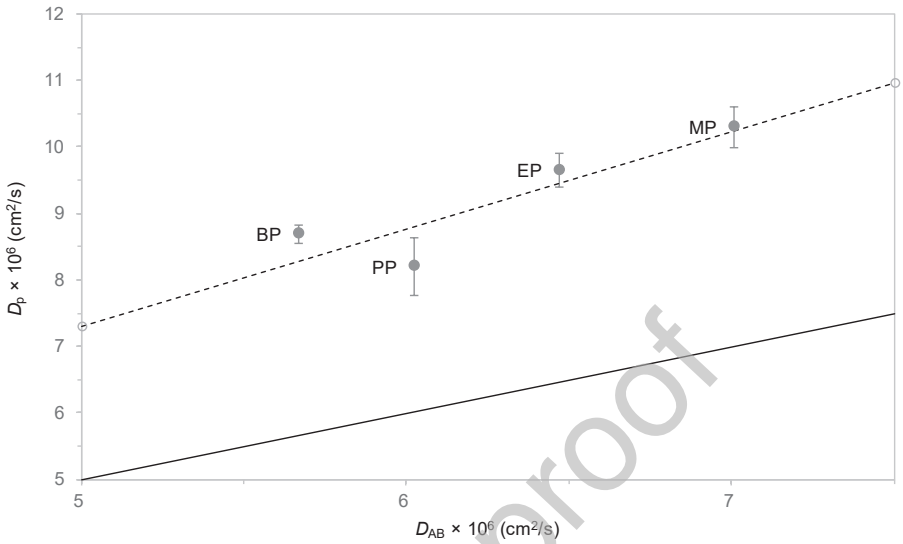

Figure 2: Plot of D_p versus D_{AB} predicted by Wilke-Chang correlation. Solid line represents diagonal. Dotted line represents the equation y=1.46x.

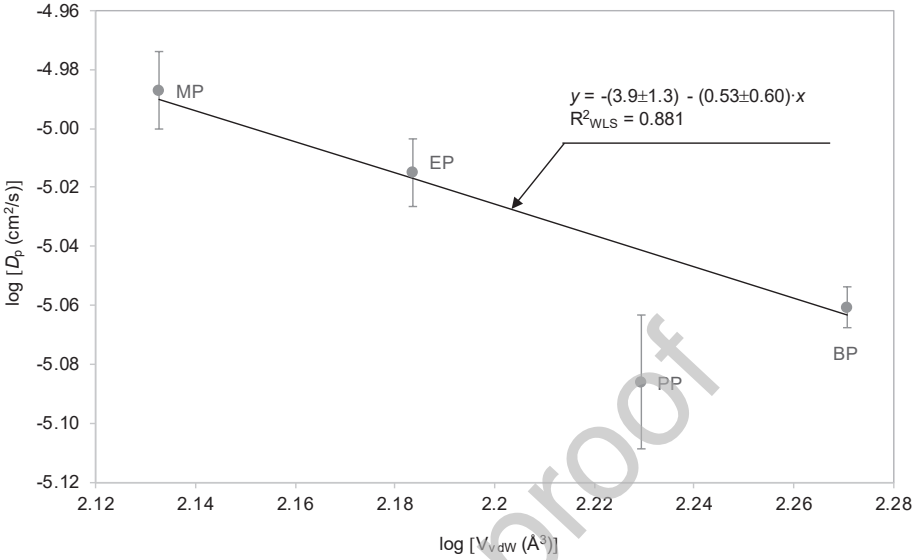

Figure 3: Log-log plot of D_p versus van der Waals volume. Solid line represents weighted least-squares regression equation.

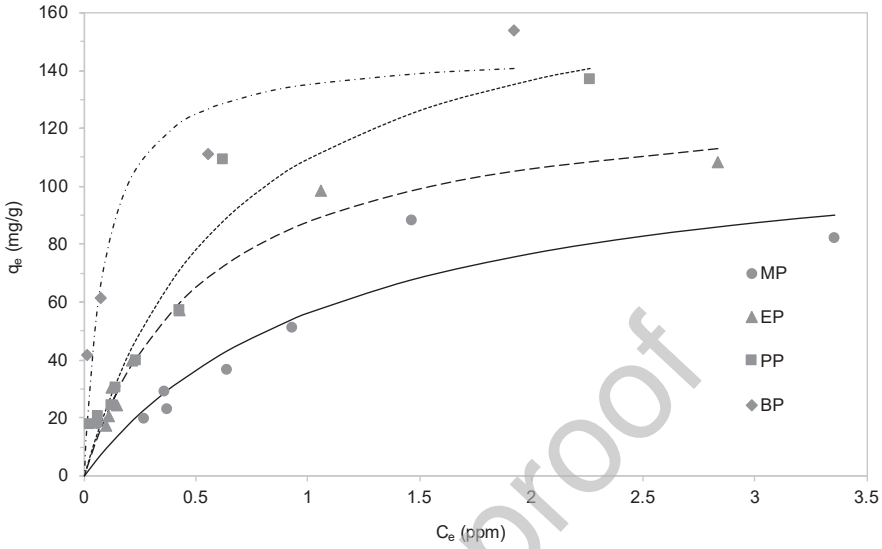

Figure 4: Effect of the paraben in adsorption isotherm. Lines represent Langmuir isotherms fitted by nonlinear least squares. *Experimental conditions*: Temperature, 20 ℃; mass of adsorbent, 10-70 mg; volume of solution, 250 mL; initial concentration of paraben, 5 mg L^{-1}.

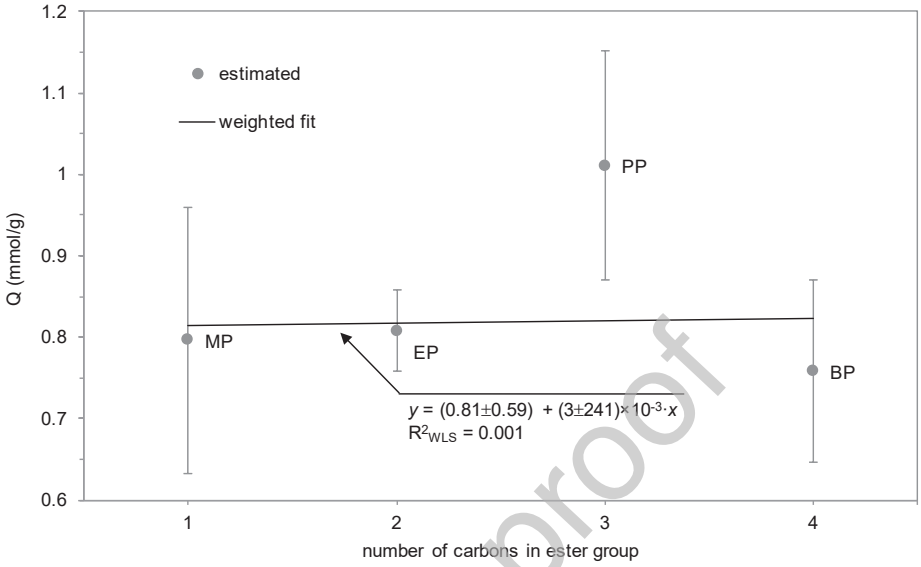

Figure 5: Monolayer capacity estimated by Langmuir isotherm as a function of alkyl ester side-chain length of paraben.

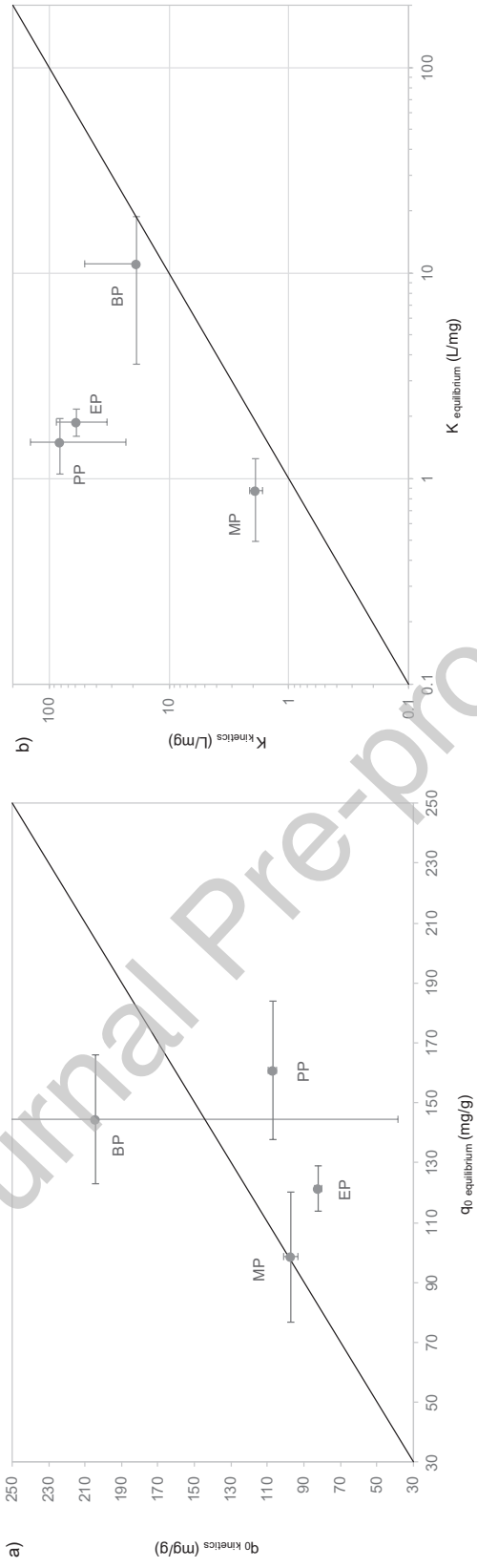

Figure 6: Comparison between equilibrium parameters calculated from the estimated values of kinetic analysis and those obtained from the equilibrium analysis for methyl- (MP), ethyl- (EP), propyl- (PP), and butylparaben (BP): a) q_0; b) K. Solid lines represent diagonals. Both horizontal and vertical error bars represent standard error of the predicted values.

CRediT author statement

Luís M. S. Silva: Supervision, Software, Validation, Writing - Original draft preparation, Writing- Reviewing and Editing

María J. Muñoz-Peña: Investigation, Validation

J.R. Dominguez: Conceptualization, Methodology

T. Gonzalez: Conceptualization, Methodology

E.M. Cuerda Correa: Writing- Original draft preparation, Validation, Writing- Reviewing and Editing

Declaration of interests

The authors declare that they have no known competing financial interests or personal relationships that could have appeared to influence the work reported in this paper.